steel research international
www.steel-research.de

Tempering and Intercritical Annealing of Air-Hardening 4 wt% Medium Manganese Steels

Alexander Gramlich and Wolfgang Bleck*

The mechanical properties after tempering and intercritical annealing of medium manganese steels with 4 wt% Mn for forging applications are presented. After forging with subsequent air cooling, heat treatments were performed, specifically tempering from 250 and 450 °C and intercritical annealing between 600 and 675 °C. Tensile properties, Charpy V-notch impact toughness, and hardness were determined and compared with microstructural features characterized by metallography and synchrotron measurements, leading to the classification of six different heat treatment stages for medium manganese steels. Furthermore, the effects of different alloying additions (boron 0.0016–0.0057 wt%, molybdenum 0.2 wt%, and aluminum 0.5 wt%) are discussed with respect to the mechanical properties. It is shown that boron increases the impact toughness more effectively in the tempering regime, while the molybdenum alloyed samples exhibit higher toughness after intercritical annealing. Most of the materials and heat treatment states follow the inverse relationship between toughness and strength, while the aluminum alloyed samples show a superior toughness after tempering.

1. Introduction

The current social–economic discussion on climate change and the striving of the European Union to reach CO_2 neutrality by 2050 pressures the forging industry to drastically reduce their energy consumption. Steel forgings are widely produced from quench and tempered (Q + T) materials, which achieve their final properties after a complex heat treatment consisting of austenization, quenching, and tempering. After the Q + T heat treatment, hard machining of the forged components might be necessary as shape distortion is induced by quenching. This causes a significant loss of material during the manufacturing of the components and adds an avoidable share to the CO_2-footprint of the final product. In addition to the Q + T steels, precipitation-hardening ferritic–pearlitic steels are widely established, which can be cooled directly from the forging heat without the need of an additional heat treatment and with less machining effort. However, the mechanical properties do not completely reach the level of Q + T steels. Several new steel concepts have been developed in the past, including modified precipitation-hardening ferritic–pearlitic steels[1] and bainitic forging steels,[2,3] but either the balance of tensile strength and impact toughness was not suitable, or the application was limited to components with small wall thicknesses. Recently, air-hardening medium manganese steels have been investigated which achieve fully martensitic microstructures by air cooling. While some of these steels show inferior impact toughness caused by manganese embrittlement,[4] new results indicate that addition of aluminum leads to an improved balance of strength and ductility after air cooling making them competitive to Q + T steels.[5] Previous studies further demonstrate the superior cyclic material behavior compared with reference alloys in the as-forged condition.[6] Furthermore, the mechanical properties of medium manganese steels can be adjusted by additional heat treatments after air cooling.[7] The high manganese content enables the intercritical annealing heat treatment (heat treatment between A_1 and A_3) apart from the classic tempering treatment (heat treatment below A_1). **Figure 1** shows the tempering treatment and the intercritical annealing treatment of an air-cooled forging steel.

1.1. Tempering of Q + T Steels

Martensitic steels achieve their very high strength levels through quenching of fully austenitic microstructures at the beginning to a fully martensitic stage after rapid cooling. The resulting martensitic microstructure is generally not suitable for application in the as-quenched state, as the material shows brittle failure with insufficient ductility and toughness. After quenching, most of the carbon is already present at dislocations or other lattice defects,[8] which was recently shown by Hutchinson et al.[9] using atomprobe tomography. Tempering is subsequently applied to the as-quenched materials to increase toughness and ductility. This tempering treatment can be subdivided into five different stages, classified by the applied temperature range or the essential mechanism.[10] The impact of the five different stages of tempering and—in addition—intercritical annealing on the mechanical properties of quenched steels are schematically

A. Gramlich, Prof. W. Bleck
Steel Institute
RWTH Aachen University
Intzestraße 1, 52072 Aachen, Germany
E-mail: alexander.gramlich@iehk.rwth-aachen.de

The ORCID identification number(s) for the author(s) of this article can be found under https://doi.org/10.1002/srin.202100180.

DOI: 10.1002/srin.202100180

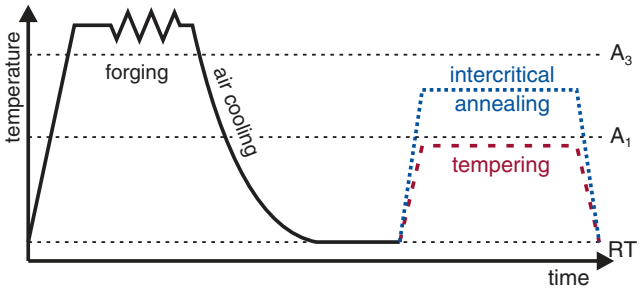

Figure 1. Comparison of tempering and intercritical annealing heat treatments of an air-cooled medium manganese forging steel.

shown in **Figure 2**, including the temperature range and the fundamental microstructural changes. The arrows indicate the change in the mechanical properties in comparison with the previous tempering stage. It must be noted that the absolute temperature values are dependent on the specific investigated alloy.

Tempering below 250 °C (stage 1) enables carbon diffusion and the formation of tiny rod-shaped carbides.[8,11,12] The precipitation of carbides leads to an increase in yield strength (YS), while the ultimate tensile strength (UTS) and the hardness stay constant or decrease slightly.[13,14]

Stage 2 covers the tempering treatments which leads to the decomposition of retained austenite to bainite, ferrite, or carbides.[8] As this process occurs parallel to other microstructural phenomena, the second tempering stage overlaps with the first and third stage.

Tempering in the temperature regime of stage 3 leads to the transformation of carbides to spheroidal carbides, mostly Fe_3C,[8,12] causing a significant drop in hardness.[14] In this temperature range, embrittlement might occur (350 °C embrittlement) through the formation of lamellar Fe_3C on grain boundaries.[8,12,15] Furthermore, this tempering stage is characterized by the maximum YS.[13]

The stage 4 of tempering generally classifies the heat treatments used for special alloyed steels, which result in secondary hardening. A significant addition of Ti, Mo, V, or W leads to the dissolution of coarse Fe_3C and to the precipitation of special alloyed carbides. Heat treatments of the fourth stage are usually performed between 500 and 600 °C.[8]

The last tempering stage (stage 5) denotes the tempering directly below A_1. This stage is characterized by the recovery of the microstructure and the formation of ferrite and spheroidal Fe_3C bringing the material close to the thermodynamic equilibrium.[12]

1.2. Intercritical Annealing of Medium Manganese Steels

Medium manganese steels (MMnS), also known as the third-generation advanced high strength steels (AHSS), have been proposed as a compromise between the first generation of AHSS (multiphase steels with ferritic matrix) and the second generation of AHSS (fully austenitic steels). The medium manganese steels are characterized by manganese contents from 4–12 wt%, which results in a multiphase structure, containing martensite, ferrite, or austenite in dependence of the process route.[16] Alloys of this kind were first proposed by Miller et al. in the 1970s[17] and have recently started to replace conventional AHSS.[18] The stabilization of austenite during intercritical annealing (IA) is achieved by the partitioning of carbon[19] and manganese[20] to the austenite phase. If silicon and aluminum are alloyed, these elements partition in the opposite direction and enrich in the ferrite phase.[21] The intercritical annealing heat treatment (per definition performed between A_1 and A_3) results in a complex microstructure of annealed martensite and austenite, which must be designed properly in accordance to achieve the desired austenite stabilities.[22] The complex microstructure is characterized by lower tensile strength and hardness in comparison with an as-quenched medium manganese steel, but the ductility

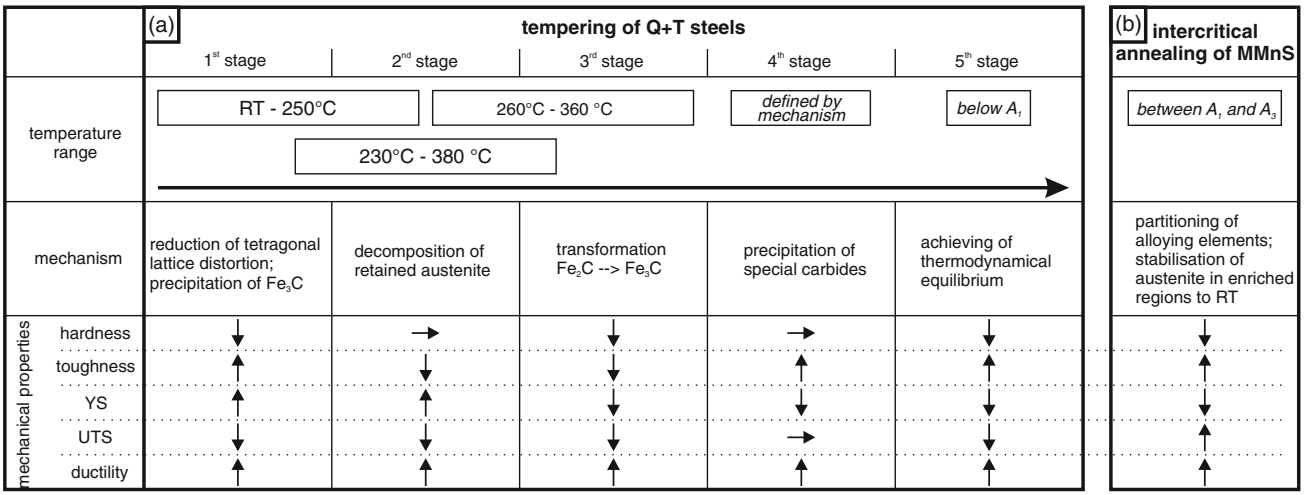

Figure 2. The figure summarizes the influence of different tempering treatments on Q + T steels as reported in the literature.[8,10–13] Different stages are classified by the temperature range, the mechanisms, and their influence on the mechanical properties compared with the as-quenched martensite properties. For comparison, the influence of an intercritical annealing heat treatment on medium manganese steels is shown as well; the mechanical properties are compared with an as-quenched medium manganese steel.[29,30]

increases significantly. The austenite grains are mechanically unstable at room temperature and can transform during plastic deformation into strain-induced martensite (transformation induced plasticity (TRIP) effect). In numerous studies, the influence of different intercritical annealing parameters on the mechanical properties has been investigated.[22–28] The utilization of the TRIP effect can increase the toughness of the steel,[29] if morphology and phase fraction of the austenite are adjusted accordingly.[7,29–31] However, the impact toughness in these steels remains a critical issue and is controversially discussed. While most of the studies attribute the embrittlement to segregations of manganese to prior austenite grain boundaries,[32–38] some authors do not report any observable segregations.[39] The effect of the segregation might be reduced by grain boundary active alloying elements such as boron[32,37] or molybdenum[33] which strengthen the grain boundaries and prevent critical manganese segregations. Another possibility of increasing the toughness is applying cold deformation before the intercritical annealing,[38] as the cold deformation eradicates the prior austenite grain boundaries through recrystallization.

The current study aims to investigate the influence of a wide range of heat treatment temperatures on the mechanical properties of a 4 wt% medium manganese steel. Furthermore, the difference between classic tempering treatment and intercritical annealing shall be highlighted.

2. Experimental Section

Five alloys were melted (80 kg) in a laboratory vacuum furnace and subsequently forged into rods. A base alloy composition of 4 wt% manganese, 0.5 wt% silicon, and carbon concentrations from 0.15 to 0.19 wt% has been chosen based on previous studies on air-hardening steels.[4] Hereby, manganese is alloyed to increase the critical cooling rate which allows to achieve martensite through air cooling. Silicon acts as a carbide precipitation restraining element and the different carbon concentrations are used to tailor the strength. In addition, 0.035 wt% niobium is alloyed to control the austenite grain size during the hot forging. To address the issue of grain boundary embrittlement, additional alloying concepts are utilized to improve the resistance against brittle fracture. Alloy +B and ++B are alloyed with boron (0.0016 and 0.0057 wt%, respectively) to increase the grain boundary strength. In addition, titanium is added to protect the boron from precipitation with nitrogen as boron nitrides. Molybdenum is used in alloy +Mo for grain boundary strengthening (0.2 wt%). Contrary to the +B and ++B materials, no titanium is necessary in this concept. For the +Al alloy (0.5 wt %), boron (0.003 wt%) and molybdenum (0.2 wt%) were added. Titanium is not needed in the +Al concept because the high aluminum concentration leads to the formation of AlN and therefore protects the boron from precipitation with nitrogen. The chemical compositions of all investigated laboratory melts are shown in **Table 1**. The ingots with the dimensions of $140 \times 140 \times 500\,mm^3$ were homogenized for 5 h at 1200 °C before being hot forged into rods of the dimensions of $60 \times 60 \times 1000\,mm^3$ in the temperature range from 1100 to 1200 °C. After forging, air cooling was applied to achieve the desired martensitic microstructure. Samples for mechanical testing were taken approximately 1 cm below the rod surface to minimize the influence of surface effects or core segregation. Each sample was heat-treated in a salt bath for 1 h at the respective tempering temperature (T_t) between 250 and 450 °C or at the intercritical annealing temperature (T_{ia}) between 600 and 675 °C. Finally, the samples were again air-cooled. Tensile tests were conducted using round specimens with a diameter of 6 mm and a gauge length of 30 mm with a constant strain rate of $0.0005\,s^{-1}$. Instrumented Charpy V-notch samples were tested at room temperature using a 300 J hammer. Hardness measurements have been done using the Vickers method[40] and a testing force of 98 N (HV10). The displayed values in this study (tensile test, Charpy V-notch, and hardness) represent the average from three parallel tests.

3. Results

3.1. Phase Fractions

Two alloys ++B and +Al have been investigated in the as-forged condition and after intercritical annealing for their phase fractions using synchrotron X-ray diffraction (SYXRD). The as-forged state of both materials consists of mainly body-centered cubic (bcc) phase and only small amounts of face-centered cubic (fcc) phase (3.07 vol% (±0.08) and 2.02 vol% (±0.04) for ++B and +Al, respectively); no cementite was observed. For intercritical annealing temperatures from 600 to 650 °C, cementite was detected with decreasing phase fractions from 2.21.1 vol% for alloy ++B and from 1.81.0 vol% for alloy +Al when T_{ia} was raised from 600 to 650 °C. The fcc fraction increases continuously with increasing T_{ia} from 2.735.2 vol% and from 1.728.9 vol% for alloys ++B and +Al, respectively. The change in the phase fraction after intercritical annealing for both alloys is shown in **Figure 3**. The overview of the obtained phase fractions and the corresponding lattice parameters for fcc and bcc are shown in **Table 2**.

Table 1. Chemical composition of the laboratory melts. All concentrations are given in wt%.

Alloy	C[a)]	Si	Mn	P	S[a)]	Al	Cr	Mo	Ti	Nb	B	N
ref.	0.17	0.50	3.96	0.010	0.009	0.027	0.11	0.02	<0.003	0.032	<0.0005	0.011
+B	0.19	0 50	4.02	0.008	0.011	0.031	0.11	0.02	0.020	0.035	0.0016	0.011
++B	0.17	0.50	3.99	0.010	0.009	0.025	0.11	0.02	0.020	0.033	0.0057	0.010
+Mo	0.15	0.49	4.02	0.011	0.009	0.027	0.12	0.20	<0.003	0.035	<0.0005	0.010
+Al	0.16	0.52	4.00	0.010	0.010	0.510	0.11	0.20	<0.003	0.037	0.0030	0.011

[a)]C, S determined with Leco combustion analyses.

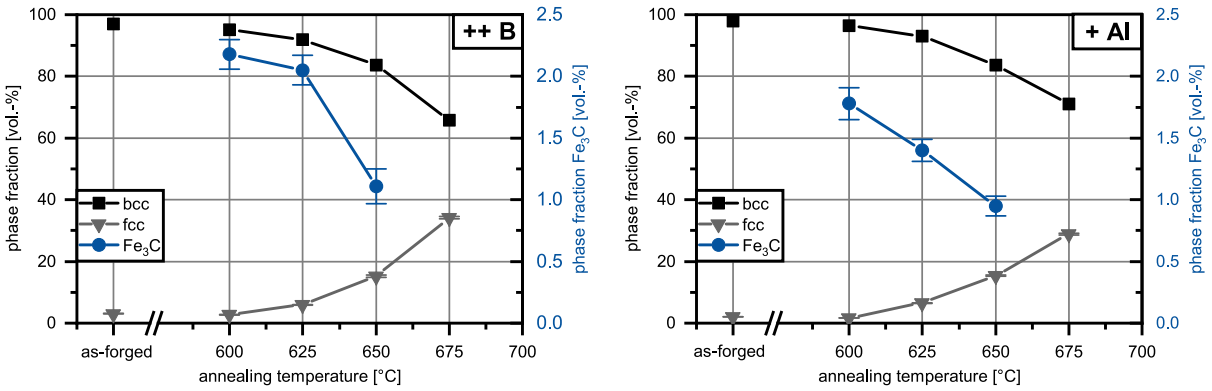

Figure 3. Phase fractions of alloys ++B and +Al in the as-forged and in the intercritically annealed state.

Table 2. Phase fractions and lattice parameters obtained by SYXRD of alloys ++B and +Al. The materials were investigated in the as-forged condition and after intercritical annealing. Errors for the lattice parameters have been omitted as they have been generally below 0.001 as well as the errors for the bcc phase which are generally below 0.01 vol%.

	Alloy ++B					Alloy +Al				
	bcc [vol%]	fcc [vol%]	Fe_3C [vol%]	a_{bcc} [Å]	a_{fcc} [Å]	bcc [vol%]	fcc [vol%]	Fe_3C [vol%]	a_{bcc} [Å]	a_{fcc} [Å]
As-forged	96.93	3.07 ± 0.08	–	2.877	3.611	97.98	2.02 ± 0.04	–	2.872	3.609
$T_{ia} = 600\,°C$	95.08	2.73 ± 0.07	2.18 ± 0.12	2.874	3.600	96.49	1.71 ± 0.05	1.78 ± 0.13	2.873	3.602
$T_{ia} = 625\,°C$	92.00	5.97 ± 0.08	2.05 ± 0.12	2.874	3.604	93.05	6.55 ± 0.07	1.40 ± 0.09	2.872	3.606
$T_{ia} = 650\,°C$	83.66	15.23 ± 0.35	1.11 ± 0.14	2.871	3.606	83.61	15.44 ± 0.20	0.95 ± 0.08	2.872	3.608
$T_{ia} = 675\,°C$	95.72	34.28 ± 0.39	–	2.872	3.605	70.07	28.92 ± 0.29	–	2.872	3.606

3.2. Tensile Tests

The yield and the tensile strength in the as-forged condition range from 918 to 993 MPa and from 1340 to 1533 MPa, while the uniform and total elongation range from 3.8% to 4.1% and from 11.8% to 12.4%. Tempering at 250 °C barely influences the UTS, A_u, and A_t; only the YS increases between 100 and 200 MPa. An increase in T_t to 350 °C does not change the YS or the elongation values of the materials in comparison with the samples tempered at $T_t = 250\,°C$, but the UTS decreases between 30 and 100 MPa. Tempering at the highest investigated T_t (=450 °C) leads to significant drops in yield and tensile strength (approximately 100 and 150 MPa), while the elongations increase between 1.3% and 4.2% for A_u and 1.6% and 3.6% for A_t.

In addition to the tempering treatments, four different temperatures in the range of intercritical annealing were investigated. The intercritical annealing with the lowest T_{ia} was performed at 600 °C. In comparison with the tempering treatment at $T_t = 450\,°C$, YS and UTS decrease for all alloys by approximately 200 MPa, while the elongations increase for most alloys except for alloy +Al. For this material, both measurements of elongation decrease by a significant amount. If T_{ia} is increased to 625 °C, only small differences for the tensile test properties can be reported, specifically a small increase in the strength values and a small decrease in the elongations was found. The strength values continue to decline slightly after a heat treatment at 650 °C, and significant increases in A_u and A_t are observed. The hottest intercritical annealing was performed at 675 °C, leading to a decrease in YS between 100 and 200 MPa accompanied by an increase in the UTS by a comparable amount. A_u increases notably for all materials, while A_t decreases or increases depending on the material. The properties obtained by the tensile tests are shown in **Table 3**.

Apart from the differences concerning the absolute values of the tensile test properties, the strain-hardening behavior changes with increasing heat treatment temperature. To address this issue, four different types of stress–strain curves are defined and shown in **Figure 4**. Type a is characteristic for the as-forged state of all investigated materials. The stress–strain curve shows a smooth transition from elastic to plastic transformation. Type b is characterized by a more abrupt transition of elastic to plastic deformation and is found for most of the tests after heat treatment in the tempering range from 250 to 450 °C. Only the molybdenum alloyed materials show this behavior also at temperatures in the intercritical annealing range (600 and 625 °C). The tensile test curves after heat treatment in the intercritical annealing range for the lower to intermediate temperatures (600–650 °C) are characterized by an inflection point at the beginning of the plastic deformation (type c). As already mentioned, the molybdenum alloyed materials are an exception from this as these alloys only developed this type of stress–strain curve after intercritical annealing at 650 °C. After intercritical annealing at 675 °C, serrated flow can be observed for all investigated materials (type d). Figure 4 shows the exemplary stress–strain curves of material ++B for all materials. The type of stress–strain curve is indicated by the superscripts in brackets. The types for the other samples are added as superscripts to the YS in Table 3.

Table 3. Overview of mechanical properties obtained by tensile test, hardness measurements, and instrumented Charpy V-notch impact test at room temperature. Yield strength (YS), ultimate tensile strength (UTS), uniform elongation (A_u), total elongation (A_t), Vickers hardness, measured Charpy energy (CVN_m), integrated Charpy energy (CVN_i), and maximum force during impact test (F_{max}) are included in the table. Superscripts "a–d" refer to the stress–strain curves type a to type d. B and pD refer to force–displacement curves of the Charpy test. "B " stands for brittle; "pD" stands for partly ductile. The properties of the as-forged condition as well as the temperatures 600–675 °C of alloys +B, ++B, and +Mo have already been published[5,7] and are shown here for the sake of completeness.

	Alloy	As-forged	250 °C	350 °C	450 °C	600 °C	625 °C	650 °C	675 °C
YS [MPa]	+B	993[a]	1182[b]	1194[b]	1081[b]	870[c]	830[c]	758[c]	635[d]
	++B	967[a]	1132[a]	1163[b]	1040[b]	838[c]	809[c]	742[c]	561[d]
	+Mo	918[a]	1101[b]	1123[b]	1045[b]	862[b]	838[b]	775[c]	592[d]
	+Al	930[a]	1070[b]	1131[b]	1062[b]	879[b]	836[b]	790[c]	695[d]
	ref	964[a]	1136[b]	1146[b]	1021[b]	844[c]	802[c]	745[c]	593[d]
UTS [MPa]	+B	1533	1469	1369	1215[b]	967	941	920	1107
	++B	1422	1409	1354	1161	943	924	900	1067
	+Mo	1374	1373	1324	1208	1006	978	951	1112
	+Al	1340	1353	1320	1214	1034	993	964	1034
	ref	1423	1401	1334	1174	966	930	932	1118
A_u [%]	+B	4.0	3.3	3.1	5.2	5.8	7.0	14.6	20.2
	++B	3.8	3.5	3.6	4.9	6.4	7.9	16.6	19.4
	+Mo	3.8	3.8	3.5	5.7	6.5	7.3	14.7	18.0
	+Al	4.1	3.5	3.0	7.2	6.6	7.3	12.4	23.7
	ref	3.9	3.4	3.2	5.3	6.0	7.1	18.0	20.7
A_t [%]	+B	12.3	12.0	11.4	14.4	15.3	17.3	24.0	26.8
	++B	12.4	12.5	12.8	14.4	16.8	18.0	27.4	26.8
	+Mo	12.2	13.1	12.8	15.5	15.6	16.4	23.8	23.4
	+Al	11.8	12.4	12.4	17.0	15.9	16.7	22.0	31.4
	ref	11.9	11.9	11.9	14.2	14.5	16.4	27.0	26.2
Hardness [HV10]	+B	452	451	421	358	299	285	261	281
	++B	442	435	417	369	309	302	294	288
	+Mo	423	420	378	411	322	315	312	301
	+Al	424	401	383	354	317	284	305	316
	Ref	418	437	422	390	308	304	293	289
CVN_m [J]	+B	15	23	6	30	23	28	85	51
	++B	25	29	18	31	22	34	82	53
	+Mo	16	19	10	21	23	35	101	62
	+Al	49	62	68	31	43	33	95	79
	ref	11	11	8	31	23	26	61	45
CVN_i [J]	+B	14	19	6	26	14	26	73	44
	++B	24	26	18	27	18	28	76	48
	+Mo	13	16	9	19	19	30	94	57
	+Al	44	49	56	22	38	29	87	73
	ref	8	9	6	28	18	24	55	41
F_{max} [kN]	+B	26.0[B]	29.3[B]	18.2[B]	27.8[B]	22.7[B]	22.6[B]	21.6[pD]	21.1[pD]
	++B	29.5[B]	30.5[B]	28.6[B]	26.3[B]	22.6[B]	23.0[B]	23.5[pD]	21.0[pD]
	+Mo	26.0[B]	27.8[B]	23.2[B]	26.9[B]	23.7[B]	23.8[B]	23.9[pD]	22.6[pD]
	+Al	27.7[pD]	29.8[pD]	29.1[pD]	27.2[B]	23.4[pD]	22.6[pD]	21.6[pD]	21.4[pD]
	ref	20.9[B]	23.0[B]	19.5[B]	27.3[B]	22.5[B]	22.6[B]	22.1[pD]	20.7[pD]

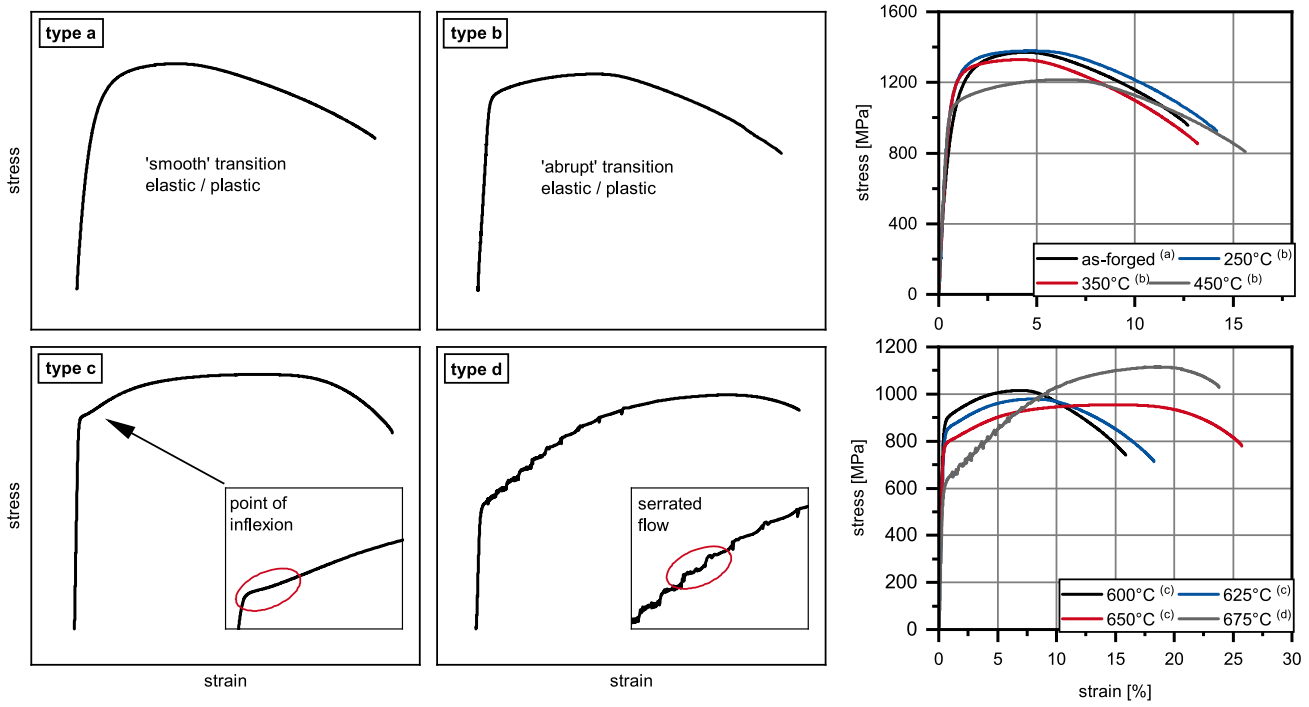

Figure 4. Classification of observed stress–strain curves for the investigated materials. In the air-cooled condition and after tempering at temperatures from 250 to 450 °C, strain hardening is characterized by continuous yielding. This continuous yielding has a smooth transition from elastic to plastic deformation in the as-forged state and gets increasingly abrupt with increasing tempering temperature. After tempering above 600 °C (intercritical annealing), discontinuous yielding takes place accompanied by a maximum in the strain-hardening curve which indicates the occurrence of TRIP effect. This effect is enhanced after tempering at 675 °C where serrated flow is observed. The stress–strain curves of alloy B++ are shown for clarification; the class of straining behavior is indicated by the superscripts in brackets.

3.3. Hardness

The hardness after tempering and intercritical annealing changes in a similar way to the UTS, reaching a maximum hardness of 452 HV10 for steel +B. Tempering and intercritical annealing lead to hardness decreases for all investigated materials. Only the reference alloy shows a small increase in hardness after tempering at $T_t = 250\,°C$ and $T_t = 350\,°C$ in comparison with the as-forged condition. While three alloys (++B, +Mo, ref) continuously decrease in hardness with increasing temperature up to the highest intercritical annealing temperature ($T_{ia} = 675\,°C$), two alloys show a minimum in hardness followed by a continuous increase (+B, +Al; 261 HV10 at 650 °C and 284 HV10 at 625 °C, respectively). All obtained hardnesses are shown in Table 3.

3.4. Instrumented Charpy V-Notch Impact Tests

The measured Charpy impact energy (CVN_m) values reveal that tempering influences the alloys in different ways. Tempering at 250 °C increases the impact energy for all alloys apart from the reference material which seems to be unaffected by tempering. However, the observed changes in CVN_m are rather small (between 313 J for alloys +Mo and +Al, respectively). If tempering is performed at 350 °C, the absorbed impact energy decreases to levels below 20 J except material +Al whose CVN further increases up to 68 J. The highest T_t leads to a bisection of the impact energy of alloy +Al, while all other alloys show an improved impact toughness between 21 and 31 J. Heat treatment in the range of intercritical annealing only shows minor effects if comparably low T_{ia} of 600 or 625 °C is used. Intercritial annealing at 650 °C increases the impact toughness of all investigated alloys between 94% and 567% (for alloys +Al and +B, respectively) in comparison with the as-forged condition. A further increase in T_{ia} decreases the absorbed impact energy again, but the values are still much higher in comparison with the as-forged state. In addition to the measured CVN_m values, the force–displacement curves have been monitored and by integration the impact energy values (CVN_i) have been determined. There are only minor differences between CVN_m and CVN_i; the temperature dependencies of both values are identical. All values for CVN_m and CVN_i are shown in Table 3. The remarkable toughness difference between the +Al and the residual alloys can also be seen in the force–displacement curve. **Figure 5** shows the force–displacement curves of the instrumented Charpy V-notch tests for alloy +Al and ++B (++B was chosen exemplary, as the curve progression is similar for alloys +B, ++B, +Mo, and ref). Alloy +Al shows a ductile fracture behavior after reaching F_{max} in the as-forged state and after tempering at 250 and 350 °C. After tempering at 450 °C, a brittle force–displacement curve with an abrupt decline of force after F_{max} can be reported. The alloys without significant additions of aluminum all show this rapid

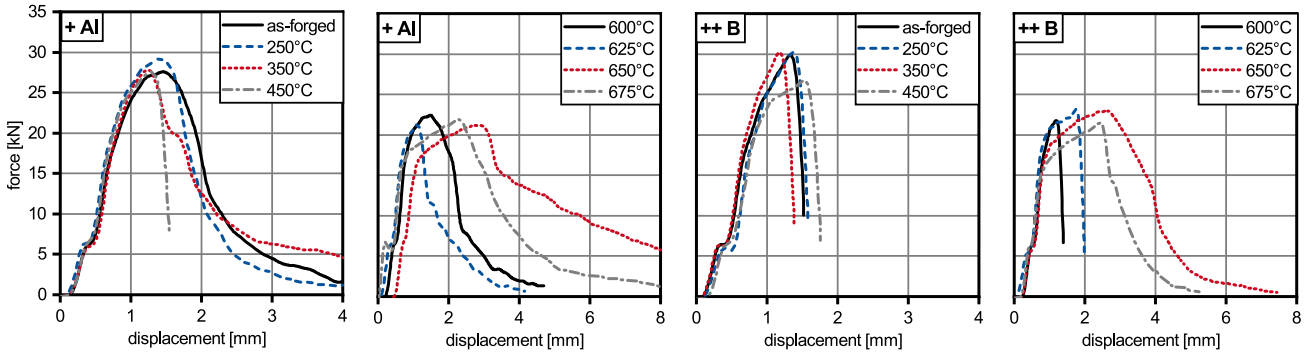

Figure 5. Force–displacement curves of alloys ++ B and + Al after tempering at different temperatures. While the maximum displacement force (F_{max}) reaches comparable levels for the aluminum and the boron alloyed sample after tempering treatment, the decline of the force after F_{max} is more rapidly for the alloy without aluminum, indicating lower ductility.

decline in the as-forged state and after tempering. Intercritical annealing leads to a reduction of F_{max} by approximately one-third of the as-forged state. However, an increase in T_{ia} leads to a change in course progression for all materials. After annealing at $T_{ia} = 650\,°C$, a very slow decline of force after F_{max} was measured leading to the highest observed impact energies. If T_{ia} is increased to 675 °C, the decline of force accelerates again, which results in lower impact energies. All values for F_{max} are shown in Table 3. The superscript B and pD indicate the type of the observed force–displacement curve (B: brittle; pD: partially ductile). The change in fracture mode can be connected to the observed fracture surfaces of the investigated alloys. The as-forged state and the tempering states of alloy ++B are characterized by small impact energies and rapid declines of the force–displacement curves as stated earlier. Mostly intergranular cleavage fracture was observed. Intercritical annealing at lower T_{ia} leads to a mixed fracture surface morphology with areas of intragranular cleavage fracture and exposed prior austenite grains. After intercritical annealing at 650 and 675 °C, only intragranular fraction can be observed, but the exposed surfaces are decorated with a secondary phase. The amount of this secondary phase increases with increasing T_{ia}. As representative examples, the different fracture surfaces of alloy ++B after tempering and intercritical annealing can be seen in **Figure 6**. While the fracture surfaces of alloy ++B can be seen as an example for alloys +B, +Mo, and ref, alloy +Al does show a completely different fracture morphology. In the as-forged state and after tempering up to 350 °C, the fracture morphology is characterized by ductile fracture with separations caused by the linear arrangement of aluminum nitrides in forging direction.[5] The sample tempered at 450 °C shows the lowest impact energy for alloy +Al and has a mixed fracture surface with regions similar to the ductile fracture surfaces of the as-forged state, but also intergranular cleavage fraction can be observed, as shown in **Figure 7**. Intercritical annealing also leads to mixture of different fracture morphologies, but contrary to the $T_t = 450\,°C$ condition, no brittle fracture is found. In addition to the ductile fracture with separations, regions similar to those reported for alloy ++B with a secondary phase on prior austenite grain boundaries are found.

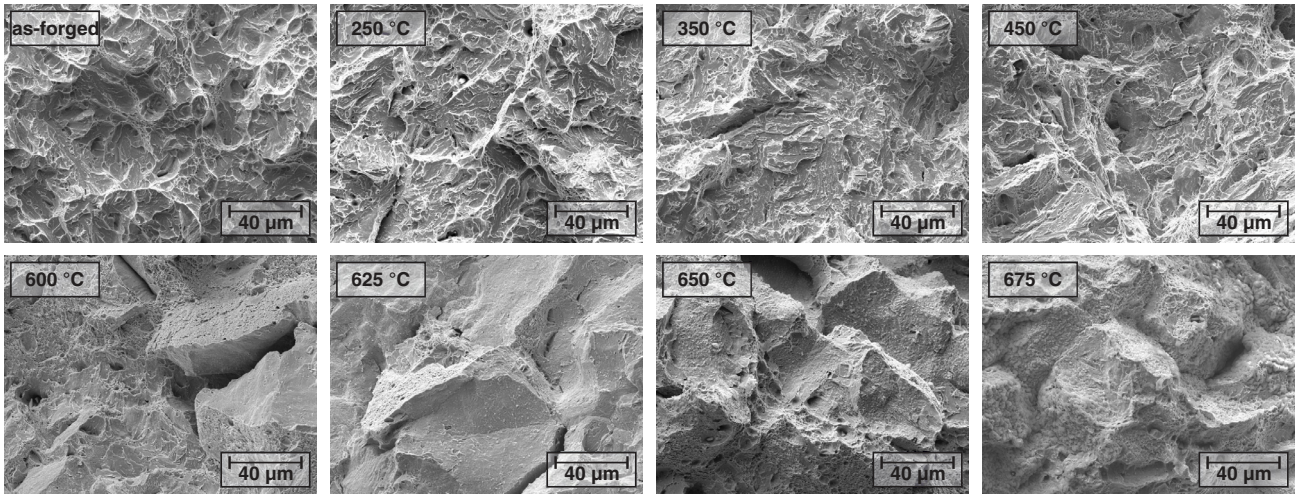

Figure 6. Fracture surface evolution of the alloy ++B after tempering with an increasing temperature. In the as-forged state and after tempering between 250 and 450 °C, the fracture surfaces show mostly intragranular cleavage fracture. After tempering at temperatures above 625 °C, cleavage fracture with partly exposed prior austenite grains is observed. These prior austenite grains are decorated with a secondary, ductile phase.

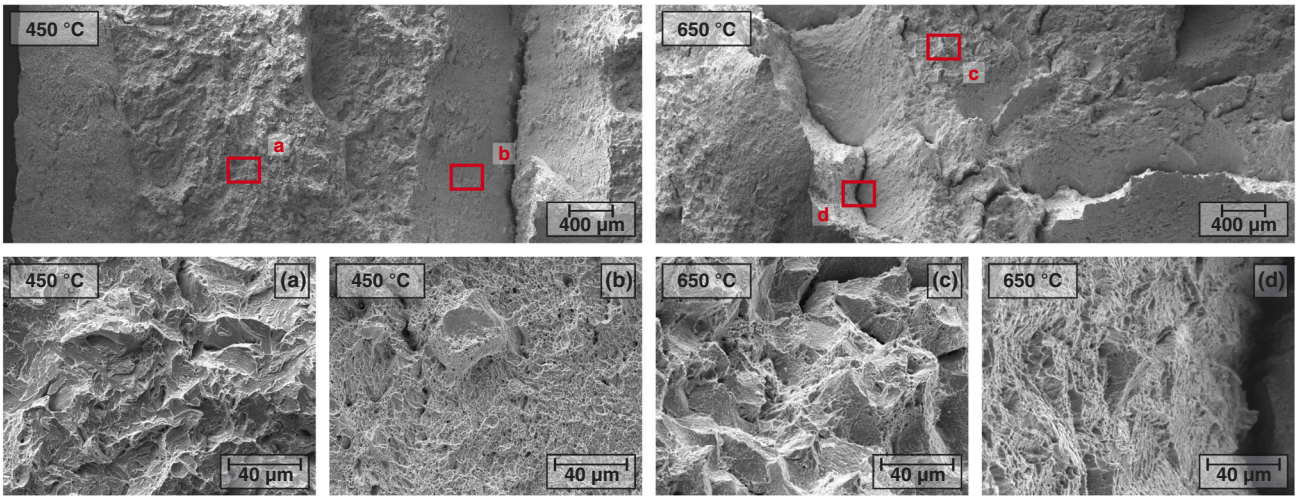

Figure 7. Fracture surfaces of Charpy V-notch impact samples of alloy +Al after a tempering at 450 and 650 °C. After tempering at 450 °C, a mixture of intragranular cleavage and shear fracture with large separations can be observed. If the tempering temperature is increased to 650 °C, the shares of cleavage fracture change to mixture of cleavage and shear fracture with partly exposed prior austenite grains similar to the other alloys, while some shear fracture with separations can still be observed.

4. Discussion

Usually, tempering of Q + T steels and intercritical annealing of medium manganese steels are considered as separate heat treatments, as they are performed on different steel classes. With air-hardening medium manganese steels, a group of materials was developed which can be exposed to tempering as well as to intercritical annealing, depending on the application and the resulting mechanical properties. Originally, these steels were designed without a consecutive heat treatment to the forging and air cooling; however, the properties can be significantly improved. Tempering and intercritical annealing have considerable effects on the mechanical properties, while different alloying elements can be used to further optimize the properties.

4.1. Classification of Tempering and Intercritical Annealing Effects

From the results of this study, tempering and intercritical annealing can each be divided into different stages, defined by the applied temperature during heat treatment (**Figure 8**). Tempering at 250 °C leads to an increase in YS, while all other properties stay more or less constant. The change in stress–strain curves from type a to type b, which accompanies the increase in YS, can be explained by the decomposition of retained austenite. The as-forged state of these materials shows austenite phase fractions between 2 and 3 vol%, as demonstrated by SYXRD. The phase fraction of austenite after intercritical annealing is slightly lower, which indicates the instability of this phase during heat treatments, which do not enable partitioning. In addition,

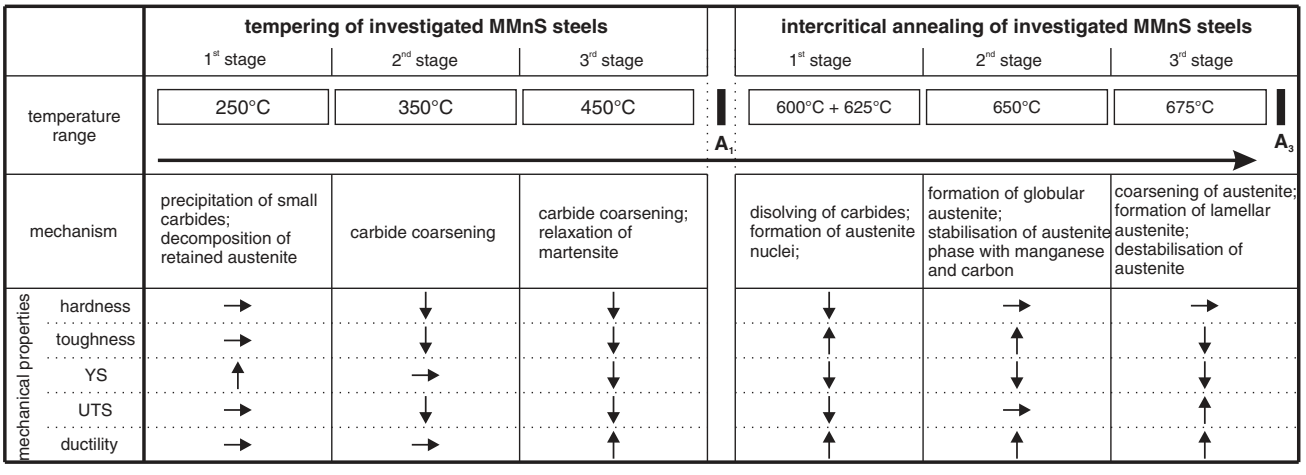

Figure 8. Chart for tempering and intercritical annealing of air-hardening medium manganese steels. Six different heat treatment stages are classified by the microstructural mechanism and their influence on the mechanical properties (indicated by arrows in comparison with the as-forged state). A temperature range is assigned to each stage.

precipitation of small carbides might take place during this heat treatment; however, as a considerable amount of very small carbides already precipitate during air cooling,[5] the effect might be negligible which explains why the hardness and the UTS are not influenced. An increase in T_t to 350 °C leads to a decrease in hardness, UTS, and impact toughness. Like standard Q + T, tempering in this temperature range leads to coarsening of carbides, which lowers the impact toughness (350 °C embrittlement) and simultaneously decreases hardness and UTS by the depletion of carbon from the matrix. These effects were observed for alloys +B, ++B, +Mo, and ref. Alloy +Al showed this behavior after tempering at 450 °C, which can be explained by the addition of aluminum, as aluminum retards the carbide growth and prevents the 350 °C embrittlement.[41] If the other alloys are tempered at 450 °C, nearly all mechanical properties decrease while the ductility increases, which is caused by further carbide coarsening and additional relaxation of the martensitic matrix. The effect of intercritical annealing on the mechanical properties strongly depends on the applied temperatures during the heat treatment. For the lower annealing temperatures of 600 and 625 °C (here summarized as first stage of intercritical annealing), further decreases in hardness and strength can be observed in comparison with the third stage of tempering. These losses are accompanied by small increases in ductility and elongation. These changes can be attributed to the continuing dissolution of carbides (as observable in SYXRD) and the stabilization of austenite during the intercritical annealing by partitioning. If the T_{ia} reaches an optimum (in this study 650 °C), globular austenite[7] can be stabilized at prior austenite grain boundaries of the martensitic matrix which increases ductility and toughness, while hardness and UTS stay at comparable levels. Exceeding the optimum T_{ia} leads to austenite coarsening during IA and the morphology changes from globular to lamelar and consecutively to a reduction of toughness.[7] The high phase fractions of austenite after intercritical annealing at this temperature lead to a pronounced TRIP effect as shown in Figure 4, which causes higher UTS and higher elongations in comparison with the $T_{ia} = 650$ °C condition. Chen et al. reported as well that the impact toughness varies in dependence of the intercritical annealing treatment. They concluded that the decrease in impact toughness after the transition of the optimum heat treatment temperature might be caused by the formation of less stable austenite and the formation of fresh martensite.[31] In contrast, recent studies suggest that the occurrence of serrated flow might not been caused by the TRIP effect but by the dislocation arrest model.[42]

4.2. Comparison of the Boron and the Molybdenum Concept

Boron and molybdenum are commonly used in medium manganese steels to suppress grain boundary embrittlement through manganese segregation. As these elements show very different diffusion and precipitation behavior, the effectiveness of boron and molybdenum strongly depends on the applied heat treatments. Boron is soluted interstitial in the austenitic matrix and therefore allows faster diffusion than molybdenum, which enables segregation at the austenite grain boundaries during air cooling. **Figure 9** shows the impact energies and the YS after

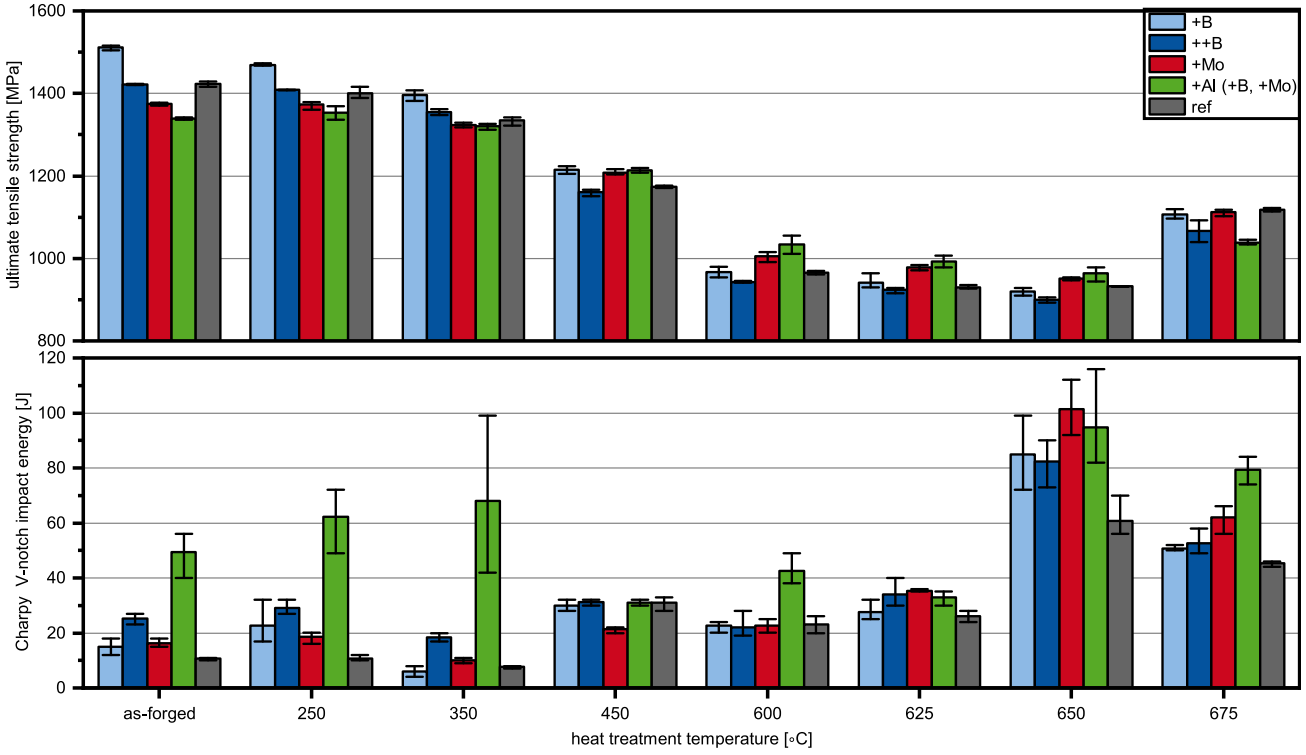

Figure 9. UTS and Charpy V-notch impact energy evolution after tempering and intercritical annealing with increasing temperatures for different alloys. The error bars indicate the minimum and maximum value obtained from the three parallel tests.

different tempering treatments of the investigated materials. The impact toughness of the boron alloyed samples exceeds the impact toughness of the molybdenum alloyed samples and the reference sample until a tempering temperature of 450 °C, showing that boron increases the toughness of the material more effectively in the tempering regime. The molybdenum alloyed samples also show a higher impact energy as the reference alloy until 350 °C but have the lowest impact energy at 450 °C. After intercritical annealing at 600 °C, no difference between the materials can be found apart from the +Al material, which is superior to the residual ones, as in the as-forged state and after tempering at 250 and 350 °C. Starting with tempering at 625 °C, molybdenum samples overtake the boron alloyed samples and achieve a 20 J higher impact toughness at 650 °C. However, if the molybdenum samples are compared with the reference alloy, air cooling and tempering at temperatures below 450 °C might have small positive effects on the Charpy impact energy. In addition to the influence on the Charpy energy, the molybdenum alloyed samples do show a different yielding behavior after tempering at elevated temperatures. As shwon in Figure 4, yielding changes from continuous yielding to pronounced yielding and finally to serrated flow. For the molybdenum free samples, the change to a pronounced YS occurs during tempering at 600 °C, while the molybdenum alloyed samples require tempering at 625 °C to produce this effect. The effect of molybdenum furthermore manifested in the higher YS after IA at 600, 625, and 650 °C. The different yielding behaviors of the laboratory melts are shown in Table 3.

4.3. Influence of Aluminum

The balance of UTS and Charpy V-notch impact energy for all investigated states, as shown in **Figure 10**, exhibits the inverse relationship between strength and toughness resulting in a banana-shaped data cloud. However, the +Al material shows a superior balance of strength and toughness in the as-forged state and in the tempering region ($T_t = 250$ °C and $T_t = 350$ °C) in comparison with the other samples. The fracture surfaces and the force–displacement curves of the Charpy samples already indicated in the as-forged state that aluminum drastically influences the fracture mechanism. While all other alloys show a more or less brittle failure during the impact test, the fracture surface of the aluminum alloyed samples does show larger amounts of ductile failure. Considering the force–displacement curves, it can be seen that for the as-forged state and temperatures up to 350 °C, only the +Al alloy shows a ductile behavior, while the other alloys show a brittle failure (Figure 5). As reported earlier,[5] this might be explained by the occurrence of pronounced in situ tempering during air cooling. The 350 °C embrittlement[8] is the reason why the temperature range of 300–400 °C is normally omitted by the industry even when desirable combinations of YS and UTS can be achieved. The embrittlement can be prevented in steels with lower manganese concentration by the addition of 0.1 wt% aluminum.[41] The observed Charpy impact energies (Table 3) demonstrate the addition of aluminum is as effective for alloys with an increased manganese concentration as in classic Q + T steels.

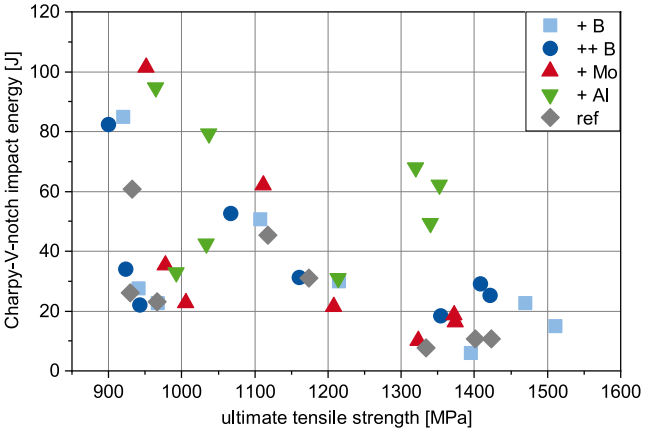

Figure 10. Balance of Charpy V-notch impact energy and UTS for the investigated materials in the as-forged and in the heat-treated conditions.

5. Conclusions

Tempering and intercritical annealing of 4 wt% broaden the achievable spectrum of strength and toughness. Due to the high alloying content, classical tempering mechanisms have to be augmented to fully describe the microstructural changes. The following conclusions can be drawn from this study: 1) Tempering and intercritical annealing of MMnS can each be categorized into three stages, classified by the heat treatment temperature. Each stage has characteristic microstructural changes and consecutively changes in the mechanical properties. 2) The addition of boron and molybdenum increases the Charpy V-notch impact energy, but the effect of each individual element is dependent on the heat treatment. While boron is effective directly after the air cooling or after tempering at low temperatures, molybdenum only increases the impact energy during intercritical annealing. 3) The stress–strain curves change from continuous yielding after air cooling and low-temperature tempering to pronounced yielding after intercritical annealing at elevated temperatures and finally to serrated flow after intercritical annealing at 675 °C. 4) The addition of molybdenum shifts the transition from continuous to pronounced yielding to higher temperatures. 5) Aluminum leads to a more ductile fracture with separations during Charpy V-notch impact tests and prevents 350 °C embrittlement in MMnS.

Acknowledgements

Results presented here are from the research project IGF 27 EWN. Funding was provided by the German Federal Ministry of Economics and Energy via the German Federation of Industrial Cooperative Research Associations Otto von Guericke (AiF) in the program to encourage the industrial Community research by a resolution of the German Bundestag and the Steel Forming Research Society (FSV).The synchrotron high-energy X-ray diffraction (HEXRD) measurements were conducted at the Powder Diffraction and Total Scattering Beamline P02.1 of PETRA III at DESY (Proposal No.: I-20191072), a member of the Helmholtz Association (HGF), which is gratefully acknowledged. Dr. Wenwen Song and Dr. Yan Ma are gratefully acknowledged for their support of acquiring HEXRD data.
Open access funding enabled and organized by Projekt DEAL.

Conflict of Interest

The authors declare no conflict of interest.

Data Availability Statement

Research data are not shared.

Keywords

forging, heat treatment, intercritical annealing, mechanical properties, medium manganese steels, tempering

Received: March 25, 2021
Revised: April 21, 2021
Published online: May 22, 2021

[1] W. Bleck, M. Bambach, V. Wirths, A. Stieben, *HTM J. Heat Treat. Mater.* **2017**, *72*, 346.
[2] C. Keul, V. Wirths, W. Bleck, *Archiv. Civil Mech. Eng.* **2012**, *12*, 119.
[3] V. Wirths, R. Wagener, W. Bleck, T. Melz, *Adv. Mater. Res.* **2014**, *922*, 813.
[4] A. Stieben, Dissertation, RWTH Aachen University, **2018**.
[5] A. Gramlich, T. Schmiedl, S. Schönborn, T. Melz, W. Bleck, *Mater. Sci. Eng. A* **2020**, *784*, 139321.
[6] T. Schmiedl, A. R. M. Gramlich, S. Schönborn, T. Melz, *Steel Res. Int.* **2020**, *91*, 2000172.
[7] A. Gramlich, R. Emmrich, W. Bleck, *Metals* **2019**, *9*, 575.
[8] G. R. Speich, W. C. Leslie, *Metall. Mater. Trans. B* **1972**, *3*, 1043.
[9] B. Hutchinson, J. Hagström, O. Karlsson, D. Lindell, M. Tornberg, F. Lindberg, M. Thuvander, *Acta Mater.* **2011**, *59*, 5845.
[10] E. Houdremont, in *Handbuch der Sonderstahlkunde*, Springer Berlin Heidelberg, Berlin, Heidelberg **1943**, 384ff.
[11] C. S. Roberts, B. L. Averbach, M. Cohen, *Trans. ASM* **1953**, *45* 576.
[12] G. R. Speich, *Trans. Metall. Soc. AIME* **1969**, *245*, 2553.
[13] H. Muir, B. L. Averbach, M. Cohen, *Trans. Am. Soc. Met.* **1955**, *47*, 380.
[14] B. S. Lement, B. L. Averbach, M. Cohen, *Trans. Am. Soc. Met.* **1954**, *46*, 851.
[15] B. S. Lement, B. L. Averbach, M. Cohen, *Trans. Am. Soc. Met.* **1955**, *47*, 291.
[16] Y. Ma, *Mater. Sci. Technol.* **2017**, *33*, 1713.
[17] R. L. Miller, *Metall. Mater. Trans. B* **1972**, *3*, 905.
[18] K. Steineder, D. Krizan, M. Schickinger, T. Hebesberger, R. Schneider, *BHM Berg- und Hüttenmännische Monatshefte* **2019**, *588*, 142.
[19] J. Speer, D. K. Matlock, B. C. de Cooman, J. G. Schroth, *Acta Mater.* **2003**, *51*, 2611.
[20] E. de Moor, D. K. Matlock, J. G. Speer, M. J. Merwin, *Scr. Mater.* **2011**, *64*, 185.
[21] S. Lee, B. C. de Cooman, *Metall. Mater. Trans. A* **2014**, *45*, 709.
[22] S. Lee, B. C. de Cooman, *Metall. Mater. Trans. A* **2013**, *44*, 5018.
[23] H. Luo, J. Shi, C. Wang, W. Cao, X. Sun, H. Dong, *Acta Mater.* **2011**, *59*, 4002.
[24] A. Arlazarov, M. Gouné, O. Bouaziz, A. Hazotte, G. Petitgand, P. Barges, *Mater. Sci. Eng.: A* **2012**, *542* 31.
[25] S. Kang, R. W. Hofer, J. G. Speer, D. Krizan, D. K. Matlock, E. de Moor, *Steel Res. Int.* **2018**, *89*, 1800069.
[26] A. Grajcar, A. Kilarski, A. Kozlowska, *Metals* **2018**, *8*, 929.
[27] A. Kozłowska, B. Grzegorczyk, M. Morawiec, A. Grajcar, *Materials* **2019**, *12*, 24.
[28] Y. Ma, B. Sun, A. Schökel, W. Song, D. Ponge, D. Raabe, W. Bleck, *Acta Mater.* **2020**, *200*, 389.
[29] G. Su, X. Gao, D. Zhang, L. Du, J. Hu, Z. Liu, *JOM* **2018**, *70*, 672.
[30] C. Sun, S. L. Liu, R. Misra, Q. Li, D. H. Li, *Mater. Sci. Eng. A* **2018**, *711*, 484.
[31] J. Chen, M.-Y. Lv, Z.-Y. Liu, G.-D. Wang, *Metall. Mater. Trans. A* **2016**, *47*, 2300.
[32] S. K. Hwang, J. W. Morris, *Metall. Mater. Trans. A* **1980**, *11*, 1197.
[33] S.-H. Song, R. Faulkner, P. Flewitt, *Mater. Sci. Eng. A* **2000**, *281*, 23.
[34] M. Nasim, B. C. Edwards, E. A. Wilson, *Mater. Sci. Eng. A* **2000**, *281*, 56.
[35] F. Nikbakht, M. Nasim, C. Davies, E. A. Wilson, H. Adrian, *Mater. Sci. Technol.* **2010**, *26*, 552.
[36] N. H. Heo, J. W. Nam, Y.-U. Heo, S.-J. Kim, *Acta Mater.* **2013**, *61*, 4022.
[37] M. Kuzmina, D. Ponge, D. Raabe, *Acta Mater.* **2015**, *86*, 182.
[38] J. Han, A. K. da Silva, D. Ponge, D. Raabe, S.-M. Lee, Y.-K. Lee, S.-I. Lee, B. Hwang, *Acta Mater.* **2017**, *122*, 199.
[39] K. H. Kwon, I.-C. Yi, Y. Ha, K.-K. Um, J.-K. Choi, K. Hono, K. Oh-ishi, N. J. Kim, *Scr. Mater.* **2013**, *69*, 420.
[40] R. L. Smith, G. E. Sandly, *Proc. Inst. Mech. Eng.* **1922**, *102*, 623.
[41] H. Schrader, H.-J. Wiester, H. Siepmann, *Archiv für das Eisenhüttenwesen* **1950**, *21*, 21.
[42] J.-H. Nam, S.-K. Oh, M.-h. Park, Y.-K. Lee, *Acta Mater.* **2021**, *206*, 116613.